Supporting Information

Label-Free Quantification of Small Molecule Binding to Membrane Proteins on Single Cells by Tracking Nanometer-Scale Cellular Membrane Deformation

Fenni Zhang, Wenwen Jing, Ashley Hunt, Hui Yu, Yunze Yang, Shaopeng Wang, Hong-Yuan Chen*, and Nongjian Tao*

S-1. Derivation of Eq. 1

The free energy of the cell surface can be expressed as [1, 2]

$$F = \frac{1}{2}\kappa(2H - C_0)^2 A + \gamma A + k_B \mathrm{T} \mathrm{f}(\phi)\mathrm{A} - \Lambda_1 H \phi \mathrm{A} - \Lambda_2 H(1-\phi)\mathrm{A}, \qquad \text{(S1)}$$

where the first term is bending energy (κ is the bending modulus, H is the mean membrane curvature, C_0 is the spontaneous curvature), the second term is surface tension (γ), the third term is the entropic contribution from the membrane proteins (k_B is the Boltzmann constant and T is temperature, and $\mathrm{f}(\phi)$ is a dimensionless parameter that depends on concentrations of the membrane proteins with and without bound ligand molecules), the fourth and fifth terms describe the interactions of the membrane proteins (with and without bound ligand molecules) with the lipid bilayer (Λ_1 and Λ_2 are the interaction strengths between the lipids and the membrane proteins with and without bound ligand molecules, respectively, and ϕ is the fraction of the membrane proteins with bound ligand molecules). If assuming ideal mixing, $\mathrm{f}(\phi)$ can be expressed as

$$\mathrm{f}(\phi) = \ln[\phi(1-\phi)]. \quad \text{(S2)}$$

By minimizing the free energy given by Eq. 1, we have

$$2\kappa(2H - C_0)\delta H A + \frac{1}{2}\kappa(2H - C_0)^2 \delta A + \gamma \delta A + k_B \mathrm{T} \ln[\phi(1-\phi)]\,\delta\mathrm{A} + k_B \mathrm{T}\frac{1-2\phi}{\phi(1-\phi)}\delta\phi\mathrm{A} -$$

$$\Lambda_1 \delta H \phi \mathrm{A} - \Lambda_1 H \delta\phi \mathrm{A} - \Lambda_1 H \phi \delta \mathrm{A} - \Lambda_2 \delta H (1-\phi)\mathrm{A} + \Lambda_2 H \delta\phi \mathrm{A} - \Lambda_2 H(1-\phi)\delta\mathrm{A} = 0, \quad \text{(S3)}$$

If we assume spherical cells, $\mathrm{A} = \frac{4\pi}{H^2}$, and S3 can be simplified as

$$\frac{\Delta D}{D} = -\frac{1}{2}\frac{(\Lambda_2 - \Lambda_1)H + k_B T \frac{1-2\phi}{\phi(1-\phi)}}{\frac{\kappa}{2}(2H - C_0)(-C_0) + \gamma + k_B \mathrm{T}\ln[\phi(1-\phi)] - \frac{1}{2}\Lambda_1 H\phi - \frac{1}{2}\Lambda_2 H(1-\phi)}\Delta\phi, \qquad \text{(S4)}$$

If the interaction energy between the membrane proteins and lipids is much greater than the thermal energy, k_BT, and the binding induced membrane deformation is relatively small, S4 can be simplified as,

$$\frac{\Delta D}{D} = \frac{(\Lambda_2 - \Lambda_1)H}{\kappa(2H - C_0)C_0 - 2\gamma}\Delta\phi. \quad \text{(S5)}$$

S-2. Cell Trapping Microfluidic Chip

Cell trapping was achieved with a microfluidic chip (similar to commercial AXIS™ Axon isolation device), consisting of two parallel fluidic channels (Figure S1). The two channels were separated by a wall with a linear array of micro-holes (10 μm diameter), with 50 μm spacing between two adjacent micro-holes. One channel (orange) was used to introduce cells, and the second channel (blue) served the purpose to maintain a pressure difference between the two channels to trap individual cell onto each micro-hole.

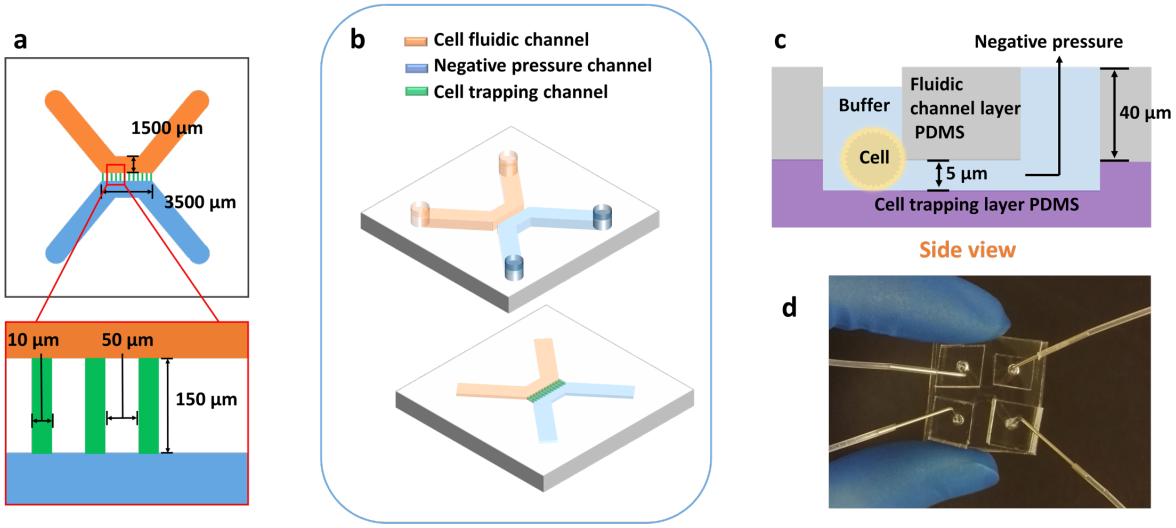

Figure S1. Microfluidic chip for single cell trapping. (a) Schematic illustration of the microfluidic chip showing two parallel fluidic channels (orange and blue). (b) Top and bottom layers of the microfluidic chip. (c) Side view of the microfluidic chip showing trapping of a cell via the micro-holes on the wall that separates the two parallel fluidic channels. (d) Photo of the microfluidic chip together with tubing connected to the inlets and outlets.

S-3. Calibration of The Differential Intensity and Cell Edge Movement

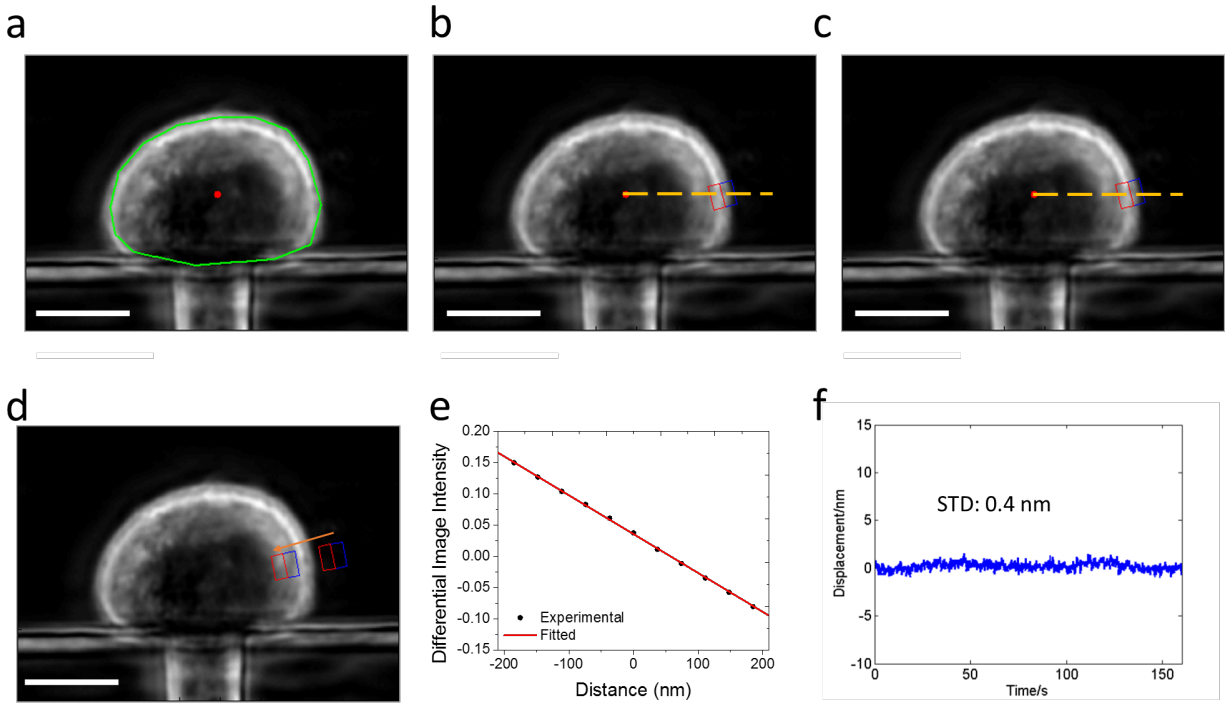

Figure S2. Calibration of the optical tracking of cellular deformation. (a) The edge (green line) and the centroid (red dot) of the cell were determined with an imaging-processing algorithm. (b) and (c) A region of interest (ROI)(1.11 μm by 2.22 μm) was selected to include the edge, and the ROI was rotated at every 1 degree along the cell edge, where the angle was defined by a radial line (from the cell centroid to the cell edge). (d) The optical tracking method was calibrated by shifting the ROI by different numbers of pixels from outside to inside of the cell in the direction

perpendicular to the tangential line at the cell edge. (e) A typical calibration curve to determine the cell deformation from the differential image intensity. (f) Noise in the measured cell deformation over time. Scale bar: 10 μm.

S-4. Measurement Error Evaluation

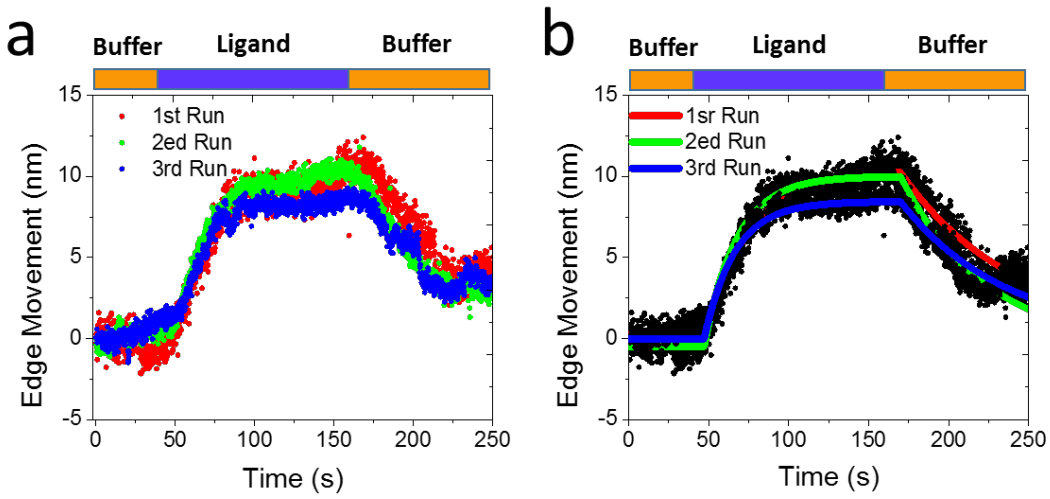

Figure S3. Repeatability of binding kinetic measurements. Binding kinetic curves of three repeated runs of acetylcholine (5 nM) binding with nAChRs on one single SH-EP_α4β2 cell. (a) Experimental data. (b) Fitted result.

Table S1. Variability of repeated binding kinetic measurements.

	$K_{on}/M^{-1}s^{-1}$	K_{off}/s^{-1}	K_D/nM
Run 1	$3.6x10^4$	$1.5x10^{-3}$	41
Run 2	$3.6x10^4$	$1.6x10^{-3}$	43
Run 3	$3.8x10^4$	$1.3x10^{-3}$	36
Mean	$3.67x10^4$	$1.47x10^{-3}$	40.0
SD	$0.12x10^4$	$0.15x10^{-3}$	3.6

S-5. Cell-to-cell Variability.

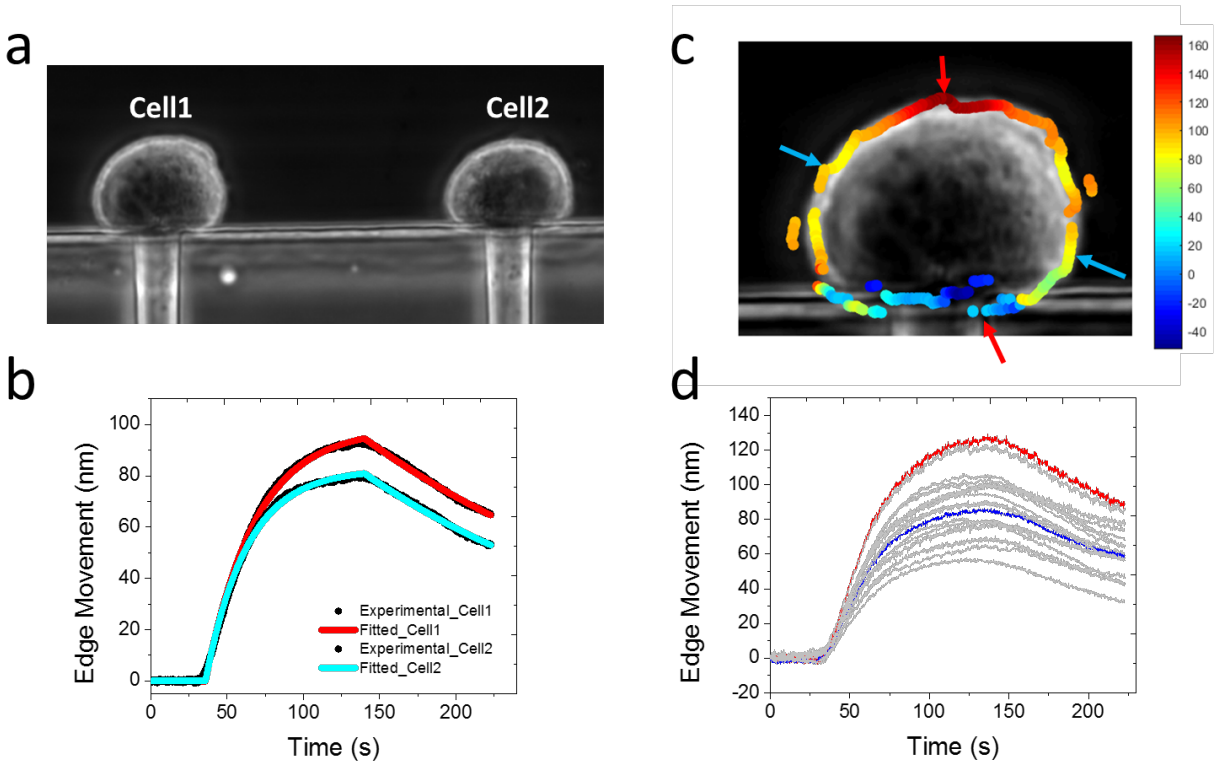

Figure S4. Variability of different cells and different regions of the same cell. (a) Phase contrast images of two wild type SH-EP1 cells. (b) Binding curves (edge movement) of two individual cells. (c) Variability in the cell deformation (edge movement) along the edge of a cell. (d) Binding curves (edge movement) of different locations along the edge of a cell.

S-6. Statistical Analysis of Cell-to-cell Variation

Table S2. Statistical analysis of the association rate constants (k_{on}), dissociation rate constants (k_{off}), and equilibrium constants (K_D) for different membrane proteins (n is cell number).

Membrane Receptors/ligands	$K_{on}/M^{-1}s^{-1}$		K_{off}/s^{-1}		K_D/nM	
	Mean	SD	Mean	SD	Mean	SD
Glycoprotein/WGA (n=10)	$2.43x10^5$	$1.94x10^5$	$4.23x10^{-3}$	$3.56x10^{-3}$	17.4	6.85
nAChRs/Acetylcholine (n=14)	$1.56x10^5$	$1.39x10^5$	$5.08x10^{-3}$	$3.69x10^{-3}$	53.7	37.4
CXCR4/AMD3100 (n=10)	$7.21x10^3$	$4.04x10^3$	$1.63x10^{-3}$	$0.70x10^{-3}$	280	184
Insulin Receptor/Insulin (n=10)	$5.07x10^4$	$3.9x10^4$	$1.44x10^{-3}$	$1.7x10^{-3}$	28.4	13.1

S-7. Cell Stiffness vs. Cell Deformation Amplitude

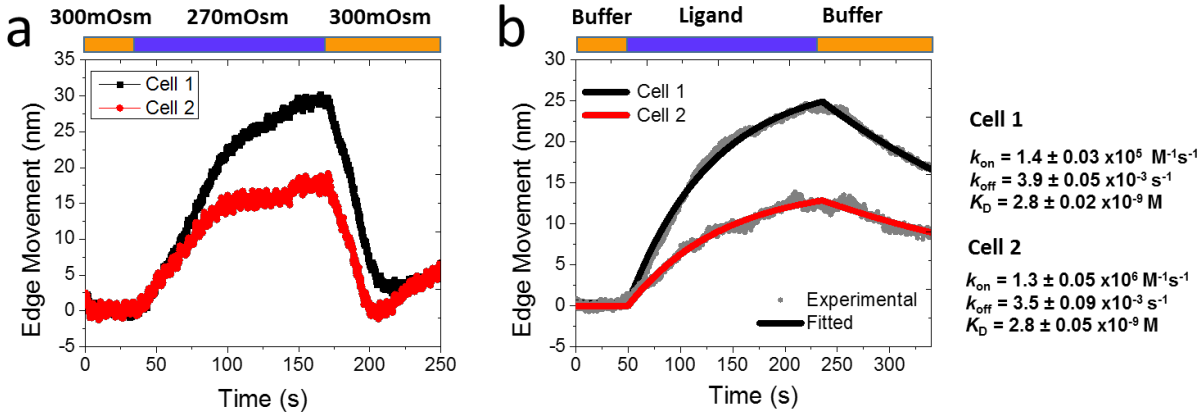

Figure S5. Dependence of binding-induced cell deformation on cell stiffness. (a) Cell edge deformation associate with osmotic pressure introduced by switching the buffer from 300 mOsm

(1X) to 270 mOsm (0.9X) PBS. (b) Cell deformation and kinetic constants associated with the binding of anti-EGFR to EGFR.

Table S3. Cell stiffness correlation of three cell pairs.

	Correlation ratio
Cell 1 – Cell 2	0.91
Cell 3 – Cell 4	0.98
Cell 5 – Cell 6	0.98
Mean	0.96
SD	0.04

S-8. Membrane Receptor Density vs. Cell Deformation Amplitude

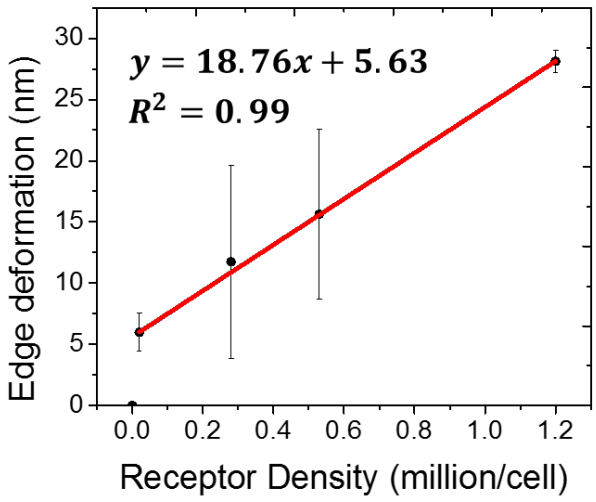

Figure S6. Linear correlation between the magnitude of the cell deformation and receptor density on cell surface. Cell deformation vs. EGFR receptor density on the cell surfaces with standard deviation of multiple cells (n=3).

S-9. Binding Kinetic Constants vs. Cell Deformation Amplitude

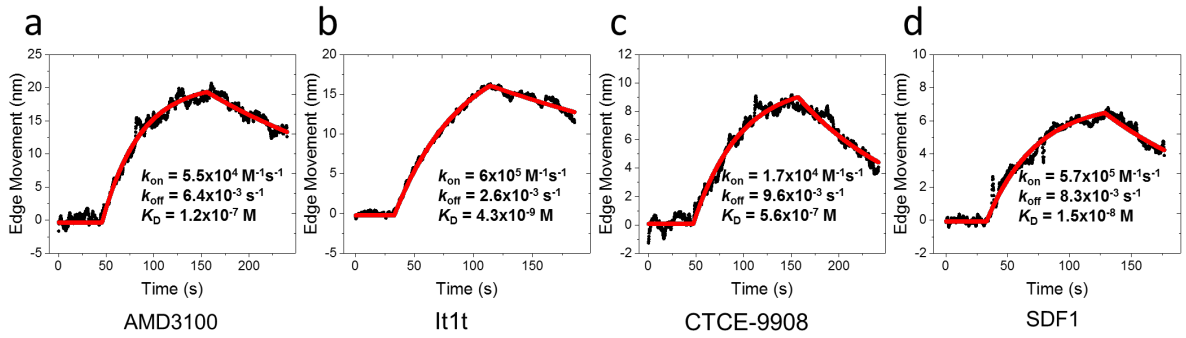

Figure S7. No correlation between the magnitude of the cell deformation and binding kinetic constants. Cell deformation and kinetic constants for (a) AMD3100-CXCR-4 binding, (b) It1t-CXCR-4 binding, (c) CTCE-9908-CXCR-4 binding, and (d) SDF1-CXCR-4 binding.

S-10. Binding Kinetics of Fixed and Living Cells

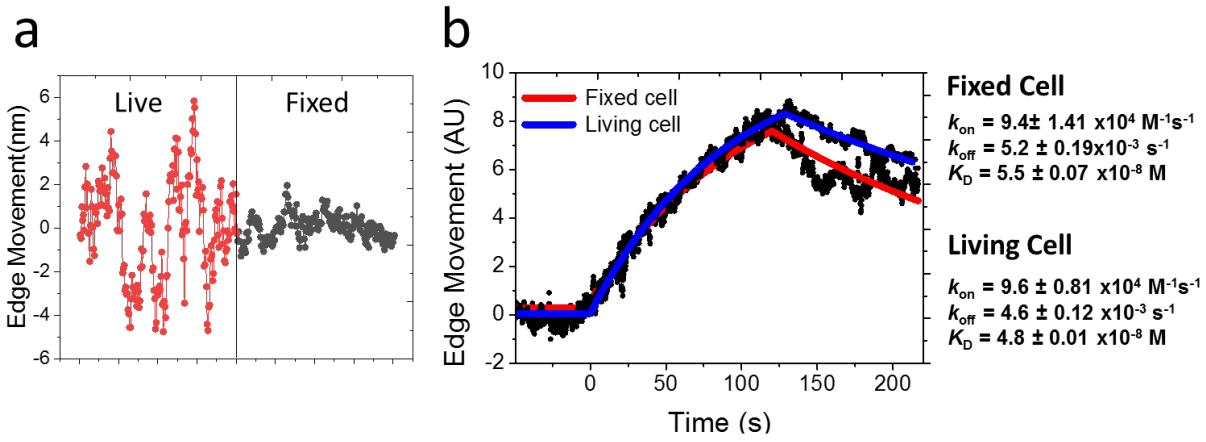

Figure S8. (a) Cell membrane fluctuation decreases after fixation. (b) Cell deformation and kinetic constants comparison for SDF-1 binding with CXCR-4 on fixed and living A549 cells.

S-11. Noise Analysis

We tracked the edge movement of a fixed object created with a marker (inset of Figure S9) with the same optical system and differential tracking algorithm, where the noise was purely due to the optical system, including light source and camera. The noise level was ~0.1 nm, several times smaller than the noise observed for cells (Figure S9). This observation suggests that the cell edge detection limit of the present system was mainly determined by the intrinsic mechanical instability of the cells.

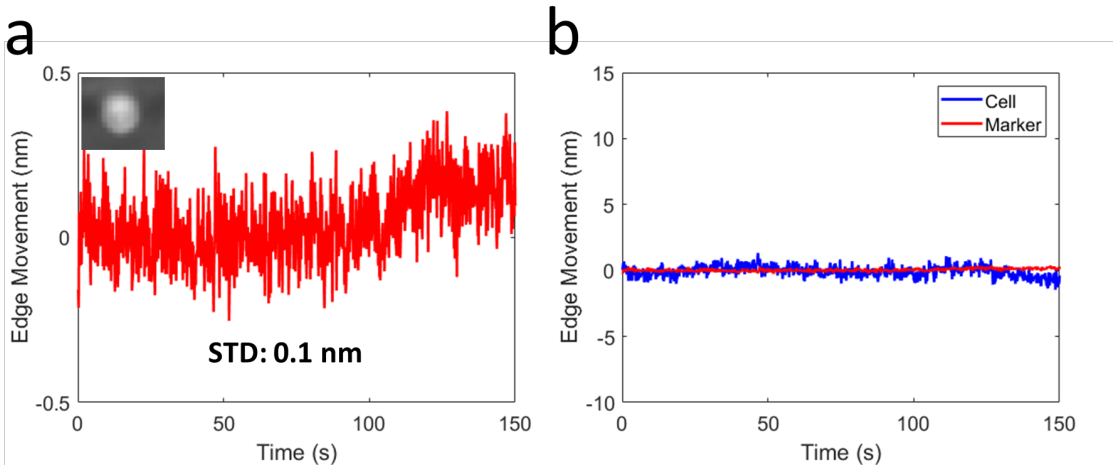

Figure S9. (a) Noise in the position (edge movement) of a fixed object (marker dot). (b) Comparison of noises in the edge movements of a cell and the marker dot.

Reference

1. Helfrich, W., Elastic Properties of Lipid Bilayers: Theory and Possible Experiments. *Z Naturforsch C* **1973,** *28*, 693-703.
2. Leibler, S., Curvature Instability in Membranes. *J Phys-Paris* **1986,** *47*, 507-516.